UC San Diego
UC San Diego Previously Published Works

Title

Size-Dependent Sigmoidal Reaction Kinetics for Pyruvic Acid Condensation at the Air-Water Interface in Aqueous Microdroplets.

Permalink

https://escholarship.org/uc/item/5vn8w2j9

Journal

Journal of the American Chemical Society, 145(41)

Authors

Li, Meng
Boothby, Christian
Continetti, Robert
et al.

Publication Date

2023-10-18

DOI

10.1021/jacs.3c08249

Peer reviewed

Communication

Size-Dependent Sigmoidal Reaction Kinetics for Pyruvic Acid Condensation at the Air−Water Interface in Aqueous Microdroplets

Meng Li, Christian Boothby, Robert E. Continetti,* and Vicki H. Grassian*

Read Online

ACCESS | Metrics & More | Article Recommendations | Supporting Information

ABSTRACT: The chemistry of pyruvic acid (PA) under thermal dark conditions is limited in bulk solutions, but in microdroplets it is shown to readily occur. Utilizing in situ micro-Raman spectroscopy as a probe, we investigated the chemistry of PA within aqueous microdroplets in a relative humidity- and temperature-controlled environmental cell. We found that PA undergoes a condensation reaction to yield mostly zymonic acid. Interestingly, the reaction follows a size-dependent sigmoidal kinetic profile, i.e., an induction period followed by reaction and then completion. The induction time is linearly proportional to the surface area (R^2), and the maximum apparent reaction rate is proportional to the surface-to-volume ratio ($1/R$), showing that both the induction and reaction occur at the air−water interface. Furthermore, the droplet size is shown to be dynamic due to changes in droplet composition and re-equilibration with the relative humidity within the environmental cell as the reaction proceeds. Overall, the size-dependent sigmoidal kinetics, shown for the first time in microdroplets, demonstrates the complexity of the reaction mechanism and the importance of the air−water interface in the pyruvic acid condensation reaction.

Aqueous microdroplets have been shown to largely enhance reaction rates and/or initiate reactions that do not occur to any great extent compared to bulk solutions.[1−16] The high surface-to-volume ratio and the unique environment at the air−water interface have been suggested as the origins of these enhanced rates.[17−21] Reactions in microdroplets of organic solvents have also been shown to be accelerated compared to bulk solutions.[22,23]

Pyruvic acid (PA) is an abundant α-keto acid in aerosols, fogs, and clouds in the atmosphere, and its conjugate base, pyruvate, is an important intermediate in several metabolic pathways.[24−27] Its oligomerization can reduce volatility and can contribute to the formation of secondary organic aerosols, impacting air quality and climate.[28,29] Although PA was reported to spontaneously form zymonic acid (ZA) in bulk solutions in the dark,[30,31] the reaction is slow, on the order of 20 days.[30] However, Petters et al.[32] found a fast volatility change during evaporation of PA in aqueous aerosols, and Kappes et al.[33] observed the formation of lactic acid and ZA after nebulizing PA solution to small charged PA droplets (60 nm in diameter).

Although there is evidence that shows enhanced reactivity of PA in microdroplets, less is known about the in situ reaction kinetics in microdroplets, and there remains a lack of understanding of the reaction kinetics and mechanisms.[34] Here we use micro-Raman spectroscopy as an in situ probe of the evolution of the chemical composition and size of PA aqueous microdroplets deposited onto hydrophobic substrates. These substrates are placed in a relative humidity (RH)- and temperature-controlled environmental cell. A schematic of the environmental cell is shown in Figure S1 and the droplet contact angle in Figure S2. Since the evaporation of H_2O from microdroplets concentrates solutes and may shift the droplet pH, these changes can contribute to enhanced reaction rates

compared to bulk solution. To investigate the intrinsic reactivity of PA in microdroplets, the RH is carefully controlled, the microdroplet is in equilibrium with H_2O vapor, and the initial PA concentration in microdroplets is controlled by the RH. All experiments, except for those investigating the influence of RH, were performed at 95% RH and 22 °C under dark conditions. High-purity nitrogen gas mixtures of wet and dry flows were used to control the RH so that the microdroplet was in equilibrium with H_2O vapor only.

Figure 1a shows the temporal changes in the Raman spectra during the dark reaction of PA in a single aqueous microdroplet on a hydrophobic substrate. The PA microdroplet is acidic with an initial pH of ca. 1, as determined by a pH calibration curve relating pH to PA concentration obtained from bulk solutions (see Figure S3); this pH is significantly lower than the pK_a of PA ($\sim$2.4 and 3.6 for keto and diol forms, respectively).[35,36] Therefore, protonated forms of PA are the major species present. The initial microdroplet radius (R_i) for this experiment was 217 μm. The error in the measured R_i is on the order of 5 μm. As can be seen in Figure 1a, there is an induction period during which no obvious changes in the spectra are detected (0 to 24 min). After the induction period, there is reaction with changes observed in the Raman spectra indicative of depletion of PA until completion after approximately 69 min, as indicated by the identical Raman spectra afterward. In particular, during the
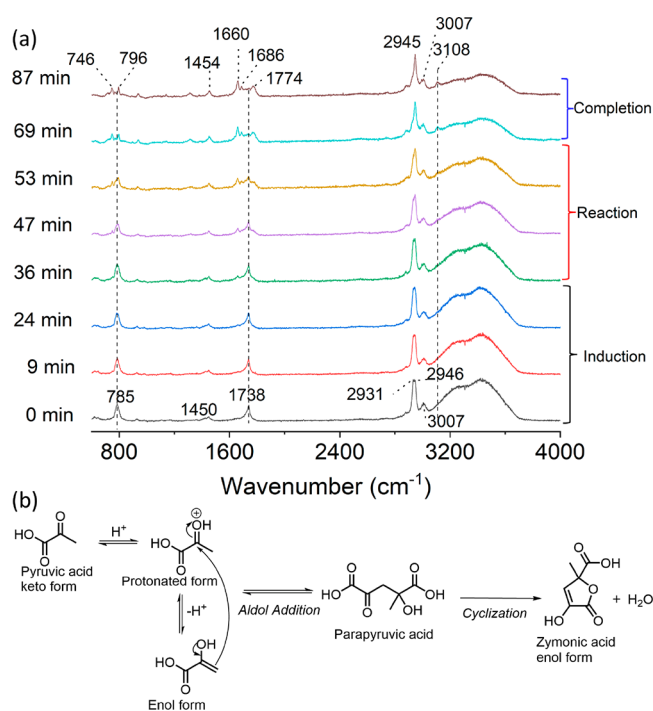
Figure 1. (a) Representative Raman spectrum change during the reaction of pyruvic acid (PA) in an acidic microdroplet with an initial radius (R_i) of 217 μm. The initial PA concentration in the microdroplet is 4.3 mol kg^{-1}. (b) Mechanism for the PA condensation reaction.[31,33,39]

reaction, Raman peaks for PA, ν(C−C) at 785 cm^{-1}, ν(C=O) at 1738 cm^{-1}, and ν(CH$_3$)$_{sym}$ of the PA keto form at 2931 cm^{-1},[37,38] decrease. Note that some PA peaks, δ(CH$_3$) at 1450 cm^{-1}, ν(CH$_3$)$_{sym}$ of the PA diol form at 2946 cm^{-1}, and

ν(CH$_3$)$_{asym}$ at 3007 cm^{-1},[37,38] do not change as much as other PA peaks, likely due to their overlap with product peaks. In addition, new peaks grow in, which are indicative of the formation of ZA. For example, the peak at 796 cm^{-1} can be assigned to ν(C−C) adjacent to the carboxylic acid group. The peaks at 1660 and 1686 cm^{-1} originate from different ν(C= C) of different forms of ZA, and peaks at 1774 and 3108 cm^{-1} are due to ν(C=O) and vinylic ν(=C−H) of ZA, respectively.[31,38] To further characterize the chemical composition of the products, we analyzed microdroplets by NMR spectroscopy and mass spectrometry. Our analysis reveals that the peaks associated with ZA dominate both the ^{1}H NMR and mass spectra, as shown in Figures S4 and S5, respectively. These results suggest that ZA is the major product. We also observed the presence of parapyruvic acid (PPA), as indicated by the small peak at m/z = 175 ([PPA − H]$^-$) in the mass spectrum. Moreover, no reactions were observed in a sodium pyruvate microdroplet (R_i = 212 μm) with a pH of ~6.8 after 12 h (Figure S6), indicating the role of acidity in the reaction mechanism. Taking these results together, we propose that the PA keto form undergoes acid-catalyzed condensation reactions, namely, aldol addition followed by cyclization, to form ZA (Figure 1b). This agrees with results obtained by Vaida and co-workers on reactions of pyruvic acid.[31,33,39]

To analyze the in situ reaction kinetics of PA in microdroplets, the PA concentration in units of molality (m_{PA}) is determined from a ratiometric approach (see the discussion in the Supporting Information (SI) and Figure S7). Figure 2a presents the time evolution of m_{PA} in a droplet with R_i = 170 μm. We observed that m_{PA} remains relatively constant during the induction period, followed by a rapid decrease and a gradual slowing down until reaction completion, i.e., PA
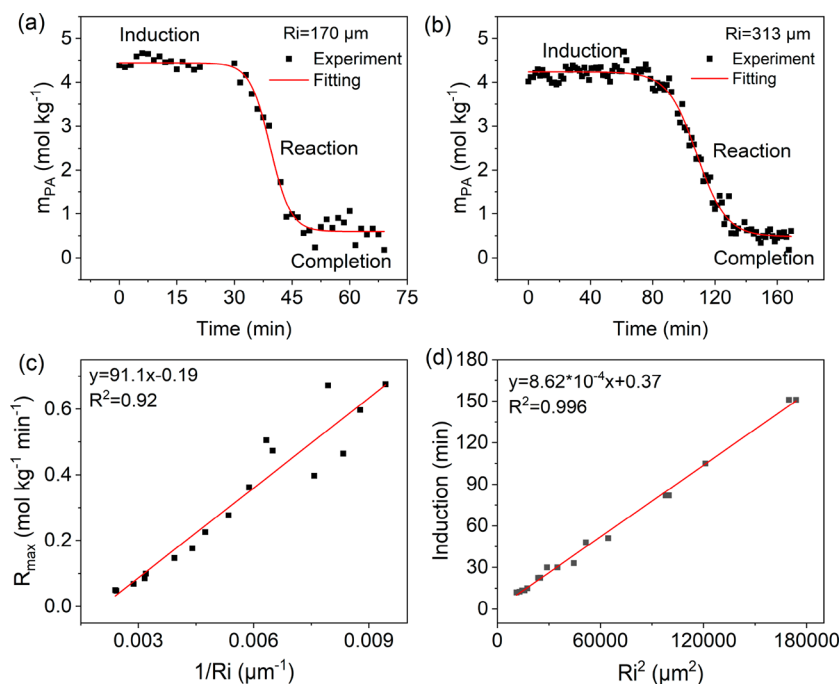

Figure 2. Size-dependent sigmoidal kinetics for PA condensation in microdroplets. (a, b) Time evolution of the PA concentration (m_{PA}) with initial radii (R_i) of (a) 170 and (b) 313 μm. The squares present experimental data, and the lines are Boltzmann sigmoidal fittings (see the SI for details of the data analysis). (c) Maximum apparent reaction rate (R_{max}) of PA versus $1/R_i$. (d) Induction time versus R_i^2. Linear fits are shown for (c) and (d).

reaction in microdroplets undergoes an induction period followed by a reaction period before completion of the reaction. For product formation, similar kinetics was observed (Figure S8). For bulk solutions, these kinetic profiles of reactant and products represent an autocatalytic reaction.[40−42]

For a larger droplet with R_i = 313 μm (Figure 2b), the kinetics is similar; however, the lengths of both the induction period and reaction period are significantly longer compared to those for droplets with R_i = 170 μm. Both the induction and reaction occur faster in the smaller droplet. The initial m_{PA} for both droplets was almost identical, as expected because the RH was the same and the initial m_{PA} is controlled by the RH. Therefore, the increased induction and reaction rate in the smaller droplets cannot be attributed to any concentration difference; instead, it arises from the difference in droplet size.

These reaction kinetics can be fit to a Boltzmann sigmoidal equation (see SI). The size-dependent sigmoidal kinetics for individual droplets covering a wide range of radii from 106 to 417 μm were analyzed. The maximum apparent reaction rate, R_{max}, as defined in eqs 1−3 in the SI, and induction time (Figure 2c,d) were determined. R_{max} of the PA reaction in microdroplets is found to be inversely proportional to R_i. It is accelerated over an order of magnitude, from 0.05 to 0.68 mol kg^{-1} min^{-1}, when R_i decreases from 417 to 106 μm. The induction time shows a linear correlation with R_i^2. These results, i.e., the surface-to-volume ratio $(1/R)$ dependence of the rate and the surface area (R^2) dependence of the induction time, definitively demonstrate that both the induction and reaction of PA condensation reactions occur at the air−water interface. The distinct environment at the air−water interface, such as the solute orientation/structure and changes in the reaction mechanism and reaction barrier, is likely the origin of the reactivity. No significant reactions were observed for bulk solutions with PA concentrations ranging from 4.7 to 141.9 mol kg^{-1} after 7 days (Figure S9). Thus, the reaction is greatly enhanced by 10^3 to 10^4 orders of magnitude, depending on the size, relative to the bulk phase.

Furthermore, droplet size is dynamic due to changes in composition and equilibration with RH in the environmental cell. As shown in Figure 3, microdroplets with R_i from 113 to 415 μm show a decrease in size over time, with smaller droplets exhibiting a higher rate of size reduction. The size evolution profile can be divided into three regions based on the rate of size decrease, i.e., a relatively low rate during the initial
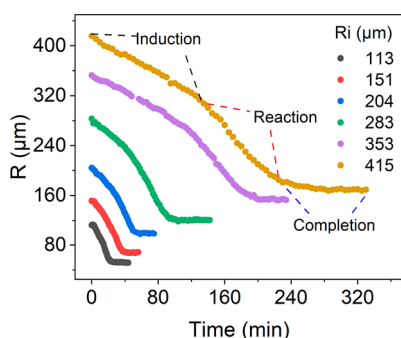
Figure 3. Representative droplet radius (R) changes as a function of time during the PA condensation reaction in microdroplets. R was determined from the bright-field image of the micro-Raman spectroscopy. The initial PA concentration in the microdroplets was in the range of 4−4.6 mol kg^{-1}.

period, followed by a higher rate and finally reaching a stable size. These three regions match the induction, reaction, and completion periods observed in the evolution of m_{PA} (Figure S10). During the induction period, both PA and H$_2$O partition from the droplet with ∼50% PA and H$_2$O loss. This is followed by reaction and changes in droplet composition with less hygroscopic products along with a re-equilibration with the RH inside of the environmental cell.[32] This leads to a decrease in microdroplet water content and size (see SI and Figure S11).

The influence of RH on the sigmoidal reaction kinetics was also investigated here by comparing the time evolution of m_{PA} under different RH conditions. In this experiment, droplets with similar R_i (210 ± 5 μm) were selected. As shown in Figure 4, we directly observed a higher initial m_{PA} (during the
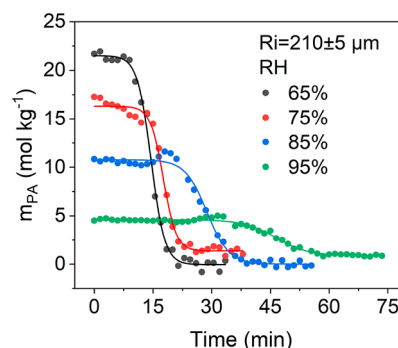
Figure 4. Comparison of the time evolution of m_{PA} under 65% (black), 75% (red), 85% (blue), and 95% (green) RH conditions. R_i = 210 ± 5 μm. The circles present experimental data, and the lines are Boltzmann sigmoidal fittings. Similar behavior of the impact of RH on microdroplets of various sizes is shown in Figure S12.

induction period) at a lower RH. This is expected as the microdroplet equilibrates with the surrounding RH, leading to different m_{PA} depending on RH.[43,44] Additionally, we observed a shorter induction period and a higher apparent reaction rate under lower-RH conditions, where the droplet has less water content. These results indicate that an increase in m_{PA} and a decrease in microdroplet water content accelerate the kinetics, both the induction and reaction.

These results taken together show that the condensation of PA under acidic conditions in microdroplets increases with decreasing microdroplet size and decreasing RH. Importantly, we find that the sigmoidal kinetics is dependent on R_i in the following manner: (1) the reaction induction time is linearly proportional to surface area (R_i^2), and (2) R_{max} is proportional to the surface-to-volume ratio $(1/R_i)$. These findings conclusively demonstrate that both the induction and reaction occur at the air−water interface. The dependence on RH shows that R_{max} increases with lower water content in the microdroplet. Most interesting is the sigmoidal kinetics, which has been observed for the first time, to the best of our knowledge, for microdroplets and, in particular, for the PA condensation reaction. Since the induction period is surface-area-dependent, it is likely that reactive complexes/species form and accumulate at the air−water interface during this period. In bulk solutions with kinetic profiles for reactants and products similar to those observed here, there is an autocatalytic reaction whereby ZA can catalyze the reaction. However, unlike bulk reactions, the loss of H$_2$O from the microdroplet as the reaction proceeds, as seen by a decrease in

droplet size, can drive the condensation reaction. The dynamic nature of the microdroplet composition, size, and surface reactivity driven in part by the gas-phase H_2O equilibrium pressure gives rise to complex reaction kinetics as demonstrated here for the first time. Further efforts to disentangle these different effects within aqueous microdroplets (water activity, droplet size, and reaction mechanisms) will be key to understanding aqueous microdroplet reactivity.

■ ASSOCIATED CONTENT

ⓢ Supporting Information

The Supporting Information is available free of charge at https://pubs.acs.org/doi/10.1021/jacs.3c08249.

> Additional information on materials and methods, including chemicals, generation of microdroplets and micro-Raman spectroscopy analysis, NMR analysis, and mass spectrometric analysis as well as the details and key advantages of the ratiometric approach, Boltzmann sigmoidal fitting, and a discussion about droplet size changes; schematic of the experimental setup (Figure S1); contact angle measurement of droplets on a hydrophobic coated surface (Figure S2); correlation between pH and PA concentration (Figure S3); NMR data (Figure S4); mass spectral data (Figure S5); Raman spectra of sodium pyruvate aqueous microdroplet from 0 to 12 h (Figure S6); calibration curve relating m_{PA} to Raman peak area (Figure S7); kinetic data demonstrating sigmoidal kinetics for both reactant depletion and product formation (Figure S8); data for bulk solutions (Figure S9); induction and reaction times as functions of droplet initial radius (Figure S10); ratio of the droplet size to the initial droplet size at the end of induction and at the end of reaction (Figure S11); time evolution of m_{PA} under different RH conditions with various droplet sizes (Figure S12) (PDF)

■ AUTHOR INFORMATION

Corresponding Authors

Vicki H. Grassian − *Department of Chemistry and Biochemistry, University of California San Diego, La Jolla, California 92093, United States;* ⓞ orcid.org/0000-0001-5052-0045; Email: vhgrassian@ucsd.edu

Robert E. Continetti − *Department of Chemistry and Biochemistry, University of California San Diego, La Jolla, California 92093, United States;* ⓞ orcid.org/0000-0002-0685-4459; Email: rcontinetti@ucsd.edu

Authors

Meng Li − *Department of Chemistry and Biochemistry, University of California San Diego, La Jolla, California 92093, United States;* ⓞ orcid.org/0000-0002-0193-5129

Christian Boothby − *Department of Chemistry and Biochemistry, University of California San Diego, La Jolla, California 92093, United States*

Complete contact information is available at:
https://pubs.acs.org/10.1021/jacs.3c08249

Notes

The authors declare no competing financial interest.

■ REFERENCES

(1) Wei, Z.; Li, Y.; Cooks, R. G.; Yan, X. Accelerated reaction kinetics in microdroplets: Overview and recent developments. *Annu. Rev. Phys. Chem.* **2020**, *71* (1), 31−51.

(2) Song, H.; Chen, D. L.; Ismagilov, R. F. Reactions in droplets in microfluidic channels. *Angew. Chem., Int. Ed.* **2006**, *45* (44), 7336−7356.

(3) Yan, X.; Bain, R. M.; Cooks, R. G. Organic reactions in microdroplets: Reaction acceleration revealed by mass spectrometry. *Angew. Chem., Int. Ed.* **2016**, *55* (42), 12960−12972.

(4) Liu, T.; Abbatt, J. P. D. Oxidation of sulfur dioxide by nitrogen dioxide accelerated at the interface of deliquesced aerosol particles. *Nat. Chem.* **2021**, *13* (12), 1173−1177.

(5) Wang, W.; Liu, M.; Wang, T.; Song, Y.; Zhou, L.; Cao, J.; Hu, J.; Tang, G.; Chen, Z.; Li, Z.; Xu, Z.; Peng, C.; Lian, C.; Chen, Y.; Pan, Y.; Zhang, Y.; Sun, Y.; Li, W.; Zhu, T.; Tian, H.; Ge, M. Sulfate formation is dominated by manganese-catalyzed oxidation of SO_2 on aerosol surfaces during haze events. *Nat. Commun.* **2021**, *12* (1), 1993.

(6) Angle, K. J.; Neal, E. E.; Grassian, V. H. Enhanced rates of transition-metal-ion-catalyzed oxidation of S(IV) in aqueous aerosols: Insights into sulfate aerosol formation in the atmosphere. *Environ. Sci. Technol.* **2021**, *55* (15), 10291−10299.

(7) Lee, J. K.; Samanta, D.; Nam, H. G.; Zare, R. N. Micrometer-sized water droplets induce spontaneous reduction. *J. Am. Chem. Soc.* **2019**, *141* (27), 10585−10589.

(8) Lee, J. K.; Walker, K. L.; Han, H. S.; Kang, J.; Prinz, F. B.; Waymouth, R. M.; Nam, H. G.; Zare, R. N. Spontaneous generation of hydrogen peroxide from aqueous microdroplets. *Proc. Natl. Acad. Sci. U.S.A.* **2019**, *116* (39), 19294−19298.

(9) Jin, S.; Chen, H.; Yuan, X.; Xing, D.; Wang, R.; Zhao, L.; Zhang, D.; Gong, C.; Zhu, C.; Gao, X.; Chen, Y.; Zhang, X. The Spontaneous electron-mediated redox processes on sprayed water microdroplets. *JACS Au* **2023**, *3* (6), 1563−1571.

(10) Wilson, K. R.; Prophet, A. M.; Rovelli, G.; Willis, M. D.; Rapf, R. J.; Jacobs, M. I. A kinetic description of how interfaces accelerate reactions in micro-compartments. *Chem. Sci.* **2020**, *11* (32), 8533−8545.

(11) Li, K.; Guo, Y.; Nizkorodov, S. A.; Rudich, Y.; Angelaki, M.; Wang, X.; An, T.; Perrier, S.; George, C. Spontaneous dark formation of OH radicals at the interface of aqueous atmospheric droplets. *Proc. Natl. Acad. Sci. U.S.A.* **2023**, *120* (15), No. e2220228120.

(12) Rao, Z.; Li, X.; Fang, Y.-G.; Francisco, J. S.; Zhu, C.; Chu, C. Spontaneous oxidation of thiols and thioether at the air−water interface of a sea spray microdroplet. *J. Am. Chem. Soc.* **2023**, *145* (19), 10839−10846.

(13) Holden, D. T.; Morato, N. M.; Cooks, R. G. Aqueous microdroplets enable abiotic synthesis and chain extension of unique peptide isomers from free amino acids. *Proc. Natl. Acad. Sci. U.S.A.* **2022**, *119* (42), No. e2212642119.

(14) Meng, Y.; Gnanamani, E.; Zare, R. N. Catalyst-free decarboxylative amination of carboxylic acids in water microdroplets. *J. Am. Chem. Soc.* **2023**, *145* (1), 32−36.

(15) Gao, D.; Jin, F.; Lee, J. K.; Zare, R. N. Aqueous microdroplets containing only ketones or aldehydes undergo Dakin and Baeyer−Villiger reactions. *Chem. Sci.* **2019**, *10* (48), 10974−10978.

(16) Chen, B.; Xia, Y.; He, R.; Sang, H.; Zhang, W.; Li, J.; Chen, L.; Wang, P.; Guo, S.; Yin, Y.; Hu, L.; Song, M.; Liang, Y.; Wang, Y.; Jiang, G.; Zare, R. N. Water−solid contact electrification causes hydrogen peroxide production from hydroxyl radical recombination in sprayed microdroplets. *Proc. Natl. Acad. Sci. U.S.A.* **2022**, *119* (32), No. e2209056119.

(17) Hao, H.; Leven, I.; Head-Gordon, T. Can electric fields drive chemistry for an aqueous microdroplet? *Nat. Commun.* **2022**, *13* (1), 280.

(18) Qiu, L.; Wei, Z.; Nie, H.; Cooks, R. G. Reaction acceleration promoted by partial solvation at the gas/solution Interface. *ChemPlusChem* **2021**, *86* (10), 1362−1365.

(19) Martins-Costa, M. T. C.; Ruiz-López, M. F. Electrostatics and chemical reactivity at the air−water interface. *J. Am. Chem. Soc.* **2023**, *145* (2), 1400−1406.

(20) Xiong, H.; Lee, J. K.; Zare, R. N.; Min, W. Strong electric field observed at the interface of aqueous microdroplets. *J. Phys. Chem. Lett.* **2020**, *11* (17), 7423−7428.

(21) Ning, A.; Zhong, J.; Li, L.; Li, H.; Liu, J.; Liu, L.; Liang, Y.; Li, J.; Zhang, X.; Francisco, J. S.; He, H. Chemical implications of rapid reactive absorption of I_2O_4 at the air-water interface. *J. Am. Chem. Soc.* **2023**, *145* (19), 10817−10825.

(22) Huang, K.-H.; Wei, Z.; Cooks, R. G. Accelerated reactions of amines with carbon dioxide driven by superacid at the microdroplet interface. *Chem. Sci.* **2021**, *12* (6), 2242−2250.

(23) Girod, M.; Moyano, E.; Campbell, D. I.; Cooks, R. G. Accelerated bimolecular reactions in microdroplets studied by desorption electrospray ionization mass spectrometry. *Chem. Sci.* **2011**, *2* (3), 501−510.

(24) Griffith, E. C.; Carpenter, B. K.; Shoemaker, R. K.; Vaida, V. Photochemistry of aqueous pyruvic acid. *Proc. Natl. Acad. Sci. U.S.A.* **2013**, *110* (29), 11714−11719.

(25) Eger, P. G.; Schuladen, J.; Sobanski, N.; Fischer, H.; Karu, E.; Williams, J.; Riva, M.; Zha, Q.; Ehn, M.; Quéléver, L. L. J.; Schallhart, S.; Lelieveld, J.; Crowley, J. N. Pyruvic acid in the boreal forest: Gas-phase mixing ratios and impact on radical chemistry. *Atmos. Chem. Phys.* **2020**, *20* (6), 3697−3711.

(26) Cody, G. D.; Boctor, N. Z.; Filley, T. R.; Hazen, R. M.; Scott, J. H.; Sharma, A.; Yoder, H. S. Primordial carbonylated iron-sulfur compounds and the synthesis of pyruvate. *Science* **2000**, *289* (5483), 1337−1340.

(27) Guzman, M. I.; Martin, S. T. Prebiotic metabolism: Production by mineral photoelectrochemistry of α-ketocarboxylic acids in the reductive tricarboxylic acid cycle. *Astrobiology* **2009**, *9* (9), 833−842.

(28) Rapf, R. J.; Perkins, R. J.; Carpenter, B. K.; Vaida, V. Mechanistic description of photochemical oligomer formation from aqueous pyruvic acid. *J. Phys. Chem. A* **2017**, *121* (22), 4272−4282.

(29) El Haddad, I.; Yao, L.; Nieto-Gligorovski, L.; Michaud, V.; Temime-Roussel, B.; Quivet, E.; Marchand, N.; Sellegri, K.; Monod, A. In-cloud processes of methacrolein under simulated conditions − Part 2: Formation of secondary organic aerosol. *Atmos. Chem. Phys.* **2009**, *9* (14), 5107−5117.

(30) Düwel, S.; Hundshammer, C.; Gersch, M.; Feuerecker, B.; Steiger, K.; Buck, A.; Walch, A.; Haase, A.; Glaser, S. J.; Schwaiger, M.; Schilling, F. Imaging of pH in vivo using hyperpolarized 13C-labelled zymonic acid. *Nat. Commun.* **2017**, *8* (1), 15126.

(31) Perkins, R. J.; Shoemaker, R. K.; Carpenter, B. K.; Vaida, V. Chemical equilibria and kinetics in aqueous solutions of zymonic acid. *J. Phys. Chem. A* **2016**, *120* (51), 10096−10107.

(32) Petters, S. S.; Hilditch, T. G.; Tomaz, S.; Miles, R. E. H.; Reid, J. P.; Turpin, B. J. Volatility change during droplet evaporation of pyruvic acid. *ACS Earth Space Chem.* **2020**, *4* (5), 741−749.

(33) Kappes, K. J.; Deal, A. M.; Jespersen, M. F.; Blair, S. L.; Doussin, J.-F.; Cazaunau, M.; Pangui, E.; Hopper, B. N.; Johnson, M. S.; Vaida, V. Chemistry and photochemistry of pyruvic acid at the air−water interface. *J. Phys. Chem. A* **2021**, *125* (4), 1036−1049.

(34) Rovelli, G.; Jacobs, M. I.; Willis, M. D.; Rapf, R. J.; Prophet, A. M.; Wilson, K. R. A critical analysis of electrospray techniques for the determination of accelerated rates and mechanisms of chemical reactions in droplets. *Chem. Sci.* **2020**, *11* (48), 13026−13043.

(35) Eugene, A. J.; Pillar-Little, E. A.; Colussi, A. J.; Guzman, M. I. Enhanced acidity of acetic and pyruvic acids on the surface of water. *Langmuir* **2018**, *34* (31), 9307−9313.

(36) Luo, M.; Shemesh, D.; Sullivan, M. N.; Alves, M. R.; Song, M.; Gerber, R. B.; Grassian, V. H. Impact of pH and NaCl and $CaCl_2$ salts on the speciation and photochemistry of pyruvic acid in the aqueous phase. *J. Phys. Chem. A* **2020**, *124* (25), 5071−5080.

(37) Reva, I. D.; Stepanian, S. G.; Adamowicz, L.; Fausto, R. Combined FTIR matrix isolation and ab initio studies of pyruvic acid: Proof for existence of the second conformer. *J. Phys. Chem. A* **2001**, *105* (19), 4773−4780.

(38) Gordon, B. P.; Moore, F. G.; Scatena, L. F.; Richmond, G. L. On the rise: Experimental and computational vibrational sum frequency spectroscopy studies of pyruvic acid and its surface-active oligomer species at the air−water interface. *J. Phys. Chem. A* **2019**, *123* (49), 10609−10619.

(39) Reed Harris, A. E.; Pajunoja, A.; Cazaunau, M.; Gratien, A.; Pangui, E.; Monod, A.; Griffith, E. C.; Virtanen, A.; Doussin, J.-F.; Vaida, V. Multiphase photochemistry of pyruvic acid under atmospheric conditions. *J. Phys. Chem. A* **2017**, *121* (18), 3327−3339.

(40) Mower, M. P.; Blackmond, D. G. Mechanistic rationalization of unusual sigmoidal kinetic profiles in the Machetti−De Sarlo cycloaddition reaction. *J. Am. Chem. Soc.* **2015**, *137* (6), 2386−2391.

(41) Blackmond, D. G. Autocatalytic models for the origin of biological homochirality. *Chem. Rev.* **2020**, *120* (11), 4831−4847.

(42) Kumar, R.; Liu, Z.; Lokitz, B.; Chen, J.; Carrillo, J.-M.; Jakowski, J.; Collier, C. P.; Retterer, S.; Advincula, R. Harnessing autocatalytic reactions in polymerization and depolymerization. *MRS Commun.* **2021**, *11* (4), 377−390.

(43) Chan, C. K.; Ha, Z.; Choi, M. Y. Study of water activities of aerosols of mixtures of sodium and magnesium salts. *Atmos. Environ.* **2000**, *34* (28), 4795−4803.

(44) Topping, D. O.; McFiggans, G. B.; Coe, H. A curved multi-component aerosol hygroscopicity model framework: Part 1 − Inorganic compounds. *Atmos. Chem. Phys.* **2005**, *5* (5), 1205−1222.